Journal of Bone and Mineral Research, 2024, **39**, 980–993
https://doi.org/10.1093/jbmr/zjae065
Advance access publication: April 23, 2024
Research Article

Single-cell RNA sequencing reveals that an imbalance in monocyte subsets rather than changes in gene expression patterns is a feature of postmenopausal osteoporosis

Lin Tao[1,*], Wen Jiang[1], Hao Li[2], Xiaochuan Wang[1], Zixuan Tian[1], Keda Yang[1,*], Yue Zhu[1,*]

[1]Department of Orthopedics, First Hospital of China Medical University, Shenyang, Liaoning, 110000, China
[2]Department of Internal Medicine, Shanghai Pudong New Area People's Hospital, Shanghai, 200000, China

*Corresponding authors: Lin Tao, Department of Orthopedics, First Hospital of China Medical University, Shenyang, Liaoning, 110000, China (taolindr@163.com); Keda Yang, Department of Orthopedics, First Hospital of China Medical University, Shenyang, Liaoning, 110000, China (terrykeda@163.com); Yue Zhu, Department of Orthopedics, First Hospital of China Medical University, Shenyang, Liaoning, 110000, China (zhuyuedr@163.com)

Abstract

The role of monocytes in postmenopausal osteoporosis is widely recognized; however, the mechanisms underlying monocyte reprogramming remain unknown. In this study, single-cell RNA sequencing (scRNA-seq) was conducted on $CD14^+$ bone marrow monocytes obtained from 3 postmenopausal women with normal BMD and 3 women with postmenopausal osteoporosis (PMOP). Monocle2 was used to classify the monocytes into 7 distinct clusters. The proportion of cluster 1 significantly decreased in PMOP patients, while the proportion of cluster 7 increased. Further analysis via GSEA, transcription factor activity analysis, and sc-metabolic analysis revealed significant differences between clusters 1 and 7. Cluster 7 exhibited upregulated pathways associated with inflammation, immunity, and osteoclast differentiation, whereas cluster 1 demonstrated the opposite results. Monocle2, TSCAN, VECTOR, and scVelo data indicated that cluster 1 represented the initial subset and that cluster 7 represents one of the terminal subsets. BayesPrism and ssGSEA were employed to analyze the bulk transcriptome data obtained from the GEO database. The observed alterations in the proportions of 1 and 7 were validated and found to have diagnostic significance. *CD16* serves as the marker gene for cluster 7, thus leading to an increased proportion of $CD16^+$ monocytes in women with PMOP. Flow cytometry was used to assess the consistency of outcomes with those of the bioinformatic analysis. Subsequently, an additional scRNA-seq analysis was conducted on bone marrow mononuclear cells obtained from 3 patients with PMOP and 3 postmenopausal women with normal BMD. The differential proportions of cluster 1 and cluster 7 were once again confirmed, with the pathological effect of cluster 7 may attribute to cell–cell communication. The scRNA-seq findings suggest that an imbalance in monocyte subsets is a characteristic feature of PMOP. These findings elucidate the limitations of utilizing bulk transcriptome data for detecting alterations in monocytes, which may influence novel research inquiries.

Keywords: postmenopausal osteoporosis, monocyte, scRNA-seq, osteoclast differentiation

Lay Summary

Monocytes are a type of white blood cell that plays a role in postmenopausal osteoporosis (PMOP), a condition where bones become weak and brittle after menopause. However, how monocytes change in this condition is not fully understood. In this study, single-cell RNA sequencing was used to analyze bone marrow monocytes from postmenopausal women with normal bone density and those with osteoporosis. Two distinct types of monocytes were identified, which were called clusters 1 and 7. In women with PMOP, there was a decrease in cluster 1 monocytes and an increase in cluster 7 monocytes. This change was validated in external datasets and in peripheral blood. Further analysis showed that cluster 7 monocytes positively correlated with inflammation, immunity, and osteoclast differentiation (a process that leads to bone resorption). Cluster 1 monocytes were found to be the initial subset, while cluster 7 monocytes were one of the terminal subsets. Overall, this study suggests that an imbalance in monocyte subsets is a characteristic feature of postmenopausal osteoporosis. These findings have important implications for understanding the role of monocytes in bone health.

Received: October 5, 2023. **Revised:** March 20, 2024. **Accepted:** April 22, 2024

Graphical Abstract

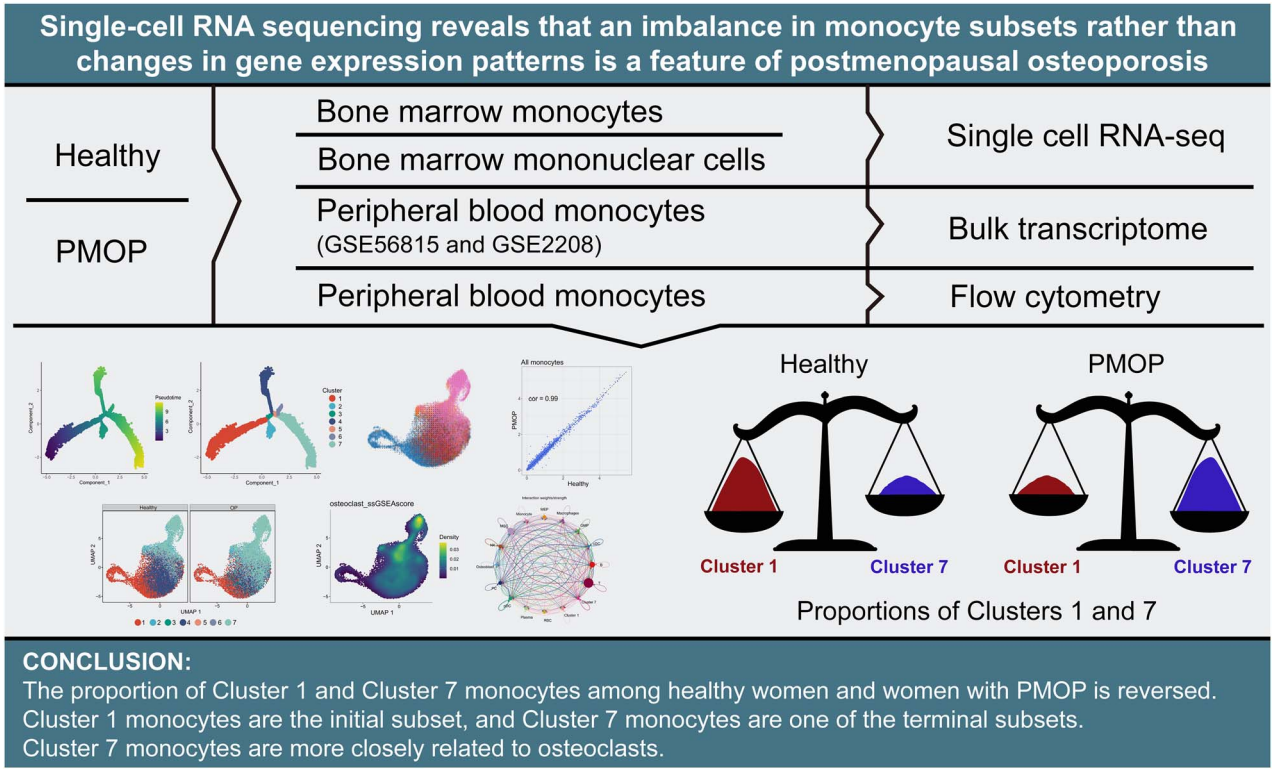

Introduction

A cross-sectional study called "China Osteoporosis Prevalence Study" showed that the prevalence of osteoporosis among postmenopausal women was 32.1% (95% CI, 30.1%–34.1%), which is much greater than that of 6.9% (95% CI, 5.8%–8.0%) in men, aged 50 yr or older.[1] For a 50-yr-old white American woman, the risk of osteoporotic fractures for the remainder of her life is estimated to be 40%, and the incidences of hip, forearm, and symptomatic vertebral fractures are 17.5%, 16.0%, and 15.6%, respectively.[2]

PMOP is a disease characterized by high bone turnover, and the increase in bone resorption is significantly greater than the increase in bone formation, leading to bone remodeling balance that is biased toward bone resorption and resulting in a gradual decrease in bone mass.[3] Osteoclasts, the only bone resorption cells, play a decisive role in the progression of pathological bone destruction.[4] Osteoclasts can be generated from monocyte–macrophage precursor cells and mature macrophages in tissue.[5] Ziegler-Heitbrock et al. identified and classified 3 human peripheral blood monocyte subsets based on expression of 2 cell surface proteins: classical monocytes ($CD14^{++}CD16-$), intermediate monocytes ($CD14^{++}CD16^{+}$), and nonclassical monocytes ($CD14^{+}CD16^{++}$).[6] In healthy human peripheral blood, classical monocytes account for approximately $84.8\% \pm 5.6\%$ of the total number of monocytes, intermediate monocytes for approximately $5.4\% \pm 1.9\%$, and nonclassical monocytes for approximately $9.2\% \pm 4.4\%$.[7] Substantial expansion of intermediate and nonclassical monocytes was observed under different inflammatory conditions[8] and correlated with enhanced bone degradation by osteoclasts.[9] An in vitro study showed that all 3 subsets of human blood monocytes can differentiate into osteoclasts and have different responses to IL-17, in which the osteoclasts produced by intermediate monocytes exhibit enhanced bone resorption activity.[10] According to a study comparing osteoclast formation in the peripheral blood between patients and healthy individuals, the number of osteoclasts formed was similar, but the resorption capacity of osteoclasts was greater in patients with osteoporosis, which suggests that peripheral osteoclast progenitor cells have the same potential for osteoclast formation but the potential to form more active osteoclasts.[11] These studies reveal that different monocyte subsets exhibit substantial functional heterogeneity; therefore, elucidating the functions of different subsets, the differentiation relationships between different subsets and the changes in different subsets is highly important for elucidating the pathogenesis of PMOP.

Bulk RNA sequencing can provide insight into only average gene expression in cells and tissues at the population level; therefore, it is difficult to explain the heterogeneity and plasticity of human bone marrow monocytes using this technique.[12] The emergence of single-cell RNA sequencing (scRNA-seq) technology provided the possibility of exploring physiological and pathological transcriptome changes at single-cell resolution, but this approach has not been applied to human bone marrow monocytes in women with PMOP.

In this study, we sequenced $CD14^{+}$ monocytes from the bone marrow of women with PMOP and healthy postmenopausal women, identified 7 monocyte clusters by Monocle2, and analyzed the functions of these clusters. We found that there was a characteristic change in the proportion of monocyte subsets in women with PMOP compared with healthy postmenopausal women, which was verified in unsorted bone marrow and peripheral blood monocytes. We

used Monocle2, TSCAN, VECTOR, and scVelo to study the differentiation relationships among the 7 clusters of bone marrow *CD14*$^+$ monocytes. We also explored cell–cell communication patterns between bone marrow cells. In addition, BayesPrism and ssGSEA were used to analyze bulk transcriptome data from the GEO database. *CD16* is a marker gene of cluster 7, and the proportion of CD16$^+$ monocytes from women with PMOP was increased. Flow cytometry was conducted, and the results were consistent with those of the bioinformatic analysis. Overall, this study provides an in-depth understanding of the specific changes occurring in cell subsets of human bone marrow *CD14*$^+$ monocytes in both healthy postmenopausal women and women with PMOP at the single-cell level, providing a new perspective for the prevention and treatment of PMOP.

Materials and methods

Sample source and preparation

Sorting of bone marrow monocytes

A total of 12 women (including 6 healthy postmenopausal women aged 55–70 yr and 6 postmenopausal women diagnosed with osteoporosis by DXA and aged 55-70 yr) signed a detailed informed consent form and were enrolled in our study. The details of the participants are shown in Table 1. The participants were admitted patients without metabolic diseases such as diabetes, fractures, or malignant masses. The bone marrow mononuclear cells of all 12 volunteers were extracted via the following method; however, cells from only 6 volunteers (3 healthy postmenopausal women and 3 postmenopausal osteoporosis patients) were sorted by CD14 microbeads, while the bone marrow mononuclear cells of the other 6 volunteers were not sorted. The density gradient centrifugation method was used to prepare a mononuclear cell suspension. Bone marrow samples were diluted with PE (PBS + EDTA) buffer (a solution containing sterile PBS [pH 7.2] and 2 mM EDTA at 2–8°C). The cell suspension was subsequently passed through a 100 μm cell filter to remove bone fragments and cell masses. Ficoll-Paque (Cytiva, 17144002) was added to the filtered suspension without mixing and the suspension was centrifuged at 445 × *g* for 35 min at 20°C. The mononuclear cell layer was undisturbed and separated from the other layers. The supernatant was removed after centrifugation at 300 × *g* for 10 min at 20°C. The cleaned cells were diluted again with PE buffer. A TC20 automated cell counter (Bio-Rad, Inc.) was used for cell counting to determine the concentration of the magnetic beads. A 5 μL cell suspension was fully mixed with trypan blue at a ratio of 1:1, and the liquid mixture was smeared onto a counting plate to determine the cell number and viability (>90%). The remaining suspension was centrifuged at 300 × *g* for 10 min, and the cell pellet was resuspended in 60 μL of PBE buffer (a solution containing PBS, pH 7.2, 0.5% bovine serum albumin [BSA], and 2 mM EDTA) per 10^7 total cells. Then, 20 μL of CD14 microbeads (Miltenyi Biotec, 130-118-906) per 10^7 cells were added and mixed well. The suspensions were incubated for 15 min at 4°C, after which 1–2 mL of PBE buffer was added to each 10^7 cells followed by centrifugation at 300 × *g* for 10 min. The cell pellets were resuspended in 500 μL of PBE (PBS + BSA + EDTA) buffer in a flow cytometry tube. CD14$^+$ monocytes were collected in a new flow cytometry tube using an automatic magnetic-activated cell sorter (AutoMACS Pro, Miltenyi Biotec).

Sorting of peripheral blood monocytes

A total of 20 women (including 10 healthy individuals aged 55–70 yr and 10 postmenopausal women diagnosed with osteopenia or osteoporosis by DXA and aged 55-70 yr) signed a detailed informed consent form and were enrolled in this study. The details of the participants are shown in Table 2. An anticoagulant tube with EDTA was used to collect 5 mL of peripheral venous blood from each volunteer, which was then spread over a lymphocyte separation solution (Solarbio, P8610). The mononuclear cell layer was extracted after centrifugation at 800 × *g* at room temperature for 20 min. Two milliliters of erythrocyte lysate (Solarbio, R1010) were added to the mononuclear cells, which were subsequently centrifuged at room temperature at 450 × *g* for 10 min after standing for 2 min. Afterward, the sediment was washed once with PBS. The cells were suspended in 80 μL of buffer, after which 20 μL of CD14 microbeads (Miltenyi Biotec, 130-118-906) was added and mixed, followed by incubation at 2–4°C for 15 min in the dark. The mixture of cells and CD14 microbeads was washed with 1–2 mL of buffer and then centrifuged at room temperature at 300 × *g* for 10 min. The cells were resuspended in 3 mL of buffer, and the cell suspension was subsequently passed through a sorting column. The sorting column was then rapidly flushed with 5 mL of buffer to obtain CD14$^+$ cells.

Library preparation and sequencing

Chromium Single cell 3′ Library and Gel Bead Kit v2 (PN-120237), Chromium Single cell 3′ Chip Kit v2 (PN-120236), and Chromium i7 Multiplex Kit (PN-120262) were used according to the manufacturer's instructions. The single-cell suspension was washed twice with 1 × PBS + 0.04% BSA. The cell number and concentration were confirmed with a TC20 automated cell counter. Approximately 8000 cells were subjected immediately to electrophoresis using a 10× Genomics Chromium Controller machine for gel beads-in-emulsion (GEM) generation. mRNA was prepared using a 10× Genomics Chromium Single cell 3′ Reagent Kit (V2 chemistry). During this step, the cells were partitioned into GEMs along with gel beads coated with oligonucleotides. These oligonucleotides provide poly-dT sequences to capture mRNAs released after cell lysis inside the droplets, as well as cell-specific and transcript-specific barcodes (16 bp 10× Barcode and 10 bp Unique Molecular Identifier, respectively). After RT-PCR, the cDNA was recovered, purified, and amplified to generate sufficient quantities for library preparation. Library quality and concentration were assessed using an Agilent Bioanalyzer 2100. The HiSeq X or NovaSeq platform for Illumina PE150 sequencing was used for the libraries. Post-processing and quality control were performed by Novogene using 10X CellRanger software (v7.1.0, 10× Genomics), and reads were aligned to the GRCh38 reference assembly (v2.2.0, 10× Genomics).

Preprocessing of single-cell data

The Fastq file from 10× Genomics was processed by CellRanger 7.1.0. Twelve "web_summary.html" files reported by Cellranger to describe the scRNA-seq data are uploaded as supplementary materials. All data analyses were performed with R (4.2.1) software unless otherwise stated. The raw count files of the single-cell data were processed using the standard procedure of the "Seurat" package.[13] Specifically,

Table 1. Bone marrow sample information.

Sample type	Group	Quantity	Age	T-score (lumbar vertebra L1–L4)
Bone marrow CD14$^+$ monocytes	Healthy	3	57, 58, 62	0.2, 0.7, 1.2
	PMOP	3	55, 61, 64	−2.5, −3.8, −2.7
Bone marrow cells	Healthy	3	55, 64, 65	−0.4, −0.4, −0.8
	PMOP	3	55, 65, 68	−3.7, −3.6, −2.9

Table 2. Peripheral blood sample information.

Sample type	Group	Quantity	Age ± SD	T-score (lumbar vertebra L1-L4) ± SD
Peripheral blood CD14$^+$ monocytes	Healthy	10	58.80 ± 6.88	0.93 ± 2.28
	Postmenopausal women diagnosed with osteopenia or osteoporosis	10	60.60 ± 5.42	−2.22 ± 0.92

when a gene was expressed in fewer than 3 cells, the gene was deleted. When the number of genes expressed in a cell was less than 500 or more than 5000, the cell was excluded. Scrublet was used in a Python environment to eliminate possible cell doublets.[14] The top 2000 highly variable genes were extracted for principal component analysis, and the top 30 principal components were used for cluster analysis. The "Harmony" method was used to remove batch effects between samples.[15] Uniform Manifold Approximation and Projection (UMAP) was utilized for dimensionality reduction. Cell clustering was determined using the "FindClusters" function with a resolution of 0.5. Celltypist was used to annotate cells according to cell surface markers.[16] The remaining nonmonocytes were deleted. The cell cycle distribution was analyzed using the "tricycle" package (version 1.4.0).[17] Specifically, the Seurat file was used as input data and first converted to a SingleCellExperiment file using the as. SingleCellExperiment function. The project_cycle_space function was subsequently used to project log counts onto the cell cycle space (with all parameters set to default values). The estimate_cycle_position function was used to estimate the cell cycle phase. 0.5 π was associated with the start of S phase, π with the start of G2M phase, 1.5 π with the middle of M phase, and 1.75 π–0.25 π with G1/G0 phase.

Pseudotime analysis

The "Monocle" package (2.24.1) was used to perform pseudotime analysis,[18] first creating the object for the proposed pseudotime analysis using the newCellDataSet function, and then selecting the highly variant genes using the detectGenes function. Finally, cell differentiation trajectories were inferred using the highly variant genes. The FindAllMarkers function of the Seurat package was used to determine the genes characteristics associated with each differentiation state. A gene was considered differentially expressed if it had a $|\log FC| > 0.25$ and an adjusted P value $<.05$. In addition, the Monocle results were reverified using the "TSCAN" R package. VECTOR[19] and scVelo[20] were used to validate the start and end points of cell differentiation. Specifically, VECTOR uses the default pipeline, the code for which is available from the website (https://github.com/jumphone/Vector). In the scVelo process, bam files after standard processing of the 10× upstream data were first converted to loom files, followed by analysis using scVelo software in a python environment, where the velocity function was used to infer rate changes. The data were finally visualized using the velocity_embedding_stream function, with all parameters set to the defaults.

Single-cell functional analysis

The VISION algorithm-based "scMetabolism" package[21] was used to perform a single-cell metabolic state analysis with a set of metabolism-related genes from the Kyoto Encyclopedia of Genes and Genomes (KEGG) database. Transcription factor activity calculations were performed using the pySCENIC.[22] Gene Set Enrichment Analysis (GSEA) was performed using the "irGSEA" R package with gene sets from the Gene Ontology database. Osteoclast scores were analyzed using ssGSEA[23] with respect to osteoclast signature (https://www.genome.jp/entry/map04380) from the KEGG database.

Bulk transcriptome data acquisition and analysis

Bulk transcriptome data were obtained from the GEO database. Monocyte samples from 20 healthy postmenopausal women with high BMD and 20 postmenopausal women with low BMD were obtained from the GSE56815 dataset (https://www.ncbi.nlm.nih.gov/geo/query/acc.cgi?acc=GSE56815); monocyte samples from 5 healthy postmenopausal women with high BMD and 5 postmenopausal women with low BMD were obtained from the GSE2208 dataset (https://www.ncbi.nlm.nih.gov/geo/query/acc.cgi?acc=GSE2208). All genes were annotated according to the gene information of the GPL96 platform. The GEOquery package was used to download and extract gene expression and clinical data.[24] Appropriate samples were selected and factoextra and FactoMineR were used for Principal Component Analysis (PCA).[25] The "limma" package was subsequently used for differentially expressed gene (DEG) analysis.[26] The ggplot2 package was used to construct a volcano plot.

Pseudobulk analysis and differential gene expression

After cluster determination, raw counts were extracted; the raw counts were aggregated to the sample level, and then DEG analysis between the healthy and disease conditions was performed. PMOP vs healthy was compared for the pseudobulk DEG analysis. Genes were deemed statistically significant if adjusted $P < .05$ and $|\log_2 FC| > 1$. Pseudobulk differential gene expression was performed using the DESeq2 package. The ggplot2 package was used to construct a volcano plot.

Deconvolution of cells in different states from single-cell data

Deconvolution of different cell states was achieved with the "BayesPrism" R package process.[27] Briefly, the cell content of different clusters from each sample in the GSE56815 dataset was evaluated based on the characteristics of the different cell states identified at the single-cell level. Specifically, according to the software usage process, we removed mitochondrial and ribosomal genes that were not meaningful for the deconvolution process. After that, only protein-coding genes were remained and analyzed by the new.prism function. To determine whether this result was biased by the algorithm, we also used the top 10 marker genes for each cluster as the signature genes and scored the cell content using ssGSEA method.[28]

Verification of cell cluster 1 and cell cluster 7 in single-cell data

We determined the presence or absence of cluster 1 cells and cluster 7 cells in the single-cell data. This process was performed using the "AUCell" R software package.[22] We performed AUCell analyses of the marker genes of the top 10 genes of cluster 1 and cluster 7 as the signature of these 2 kind of cells. The Area Under Curve (AUC) threshold was determined automatically by this algorithm.

Cell–cell communication

Cell–cell communication was analyzed using the "CellChat" package.[29] CellChat has a public repository of ligands, receptors, cofactors, and their interactions (http://www.cellchat.org/). The CellChat R package is a versatile and easy-to-use toolkit for inferring, analyzing, and visualizing cell–cell communication from any given scRNA-seq dataset. The ligand and receptor genes expressed by each cell were projected into a manually selected reference communication network, and the probability of communication in each pathway was inferred by gene expression. Finally, the netVisual_bubble function was used for visualization, with all the parameters set to the defaults.

Flow cytometry

The $CD14^+$ cells obtained using the sorting column were washed with PBS and resuspended in 1 mL of PBS, and the cell suspensions were transferred to 4 flow cytometry tubes (200 μL/tube). No antibody was added to the first tube, 5 μL of CD14 antibody (Proteintech, FITC-65056) was added to the second tube, 5 μL of CD16 antibody (Proteintech, PE-65090) was added to the third tube, and 5 μL of CD14 antibody and 5 μL of CD16 antibody were added to the fourth tube. After incubating for 15 min in the dark, flow cytometry was performed, and 10 000 cells were recorded in each tube. Flow cytometry data were processed using CytExpert 2.4. The ggstatplot was used to construct a violin plot.

Statistical methods

All statistical methods were conducted according to the corresponding R software. Difference in the proportion of $CD16^+$ monocytes between postmenopausal women diagnosed with osteopenia or osteoporosis and healthy postmenopausal women was analyzed with the Wilcoxon test. $P < .05$ was considered to indicate statistical significance.

Results

ScRNA-seq analysis revealed changes in bone marrow $CD14^+$ monocyte subsets in women with PMOP

$CD14^+$ monocytes were isolated from the bone marrow tissues of 3 women with PMOP and 3 healthy postmenopausal women. After the initial quality control evaluation (Figure S1A–F), a total of 32 252 cells were analyzed via single-cell transcriptome analysis. After sample integration, the difference in monocyte distribution between the PMOP patients and healthy postmenopausal women was visualized by the UMAP dimension reduction method (Figure 1A). The monocyte distribution between the 2 groups on the UMAP was highly consistent. A total of 7 monocyte clusters were identified by Monocle2 (cluster 1 to cluster 7) (Figure 1C). Pseudotime analysis of bone marrow monocytes was carried out by "Monocle". As shown in Figure 1B–D, the results showed that the differentiation direction among the clusters may be from cluster 1 to cluster 7. Cluster 1 is the initial cluster, differentiating at 3 nodes. It has the potential to differentiate into cluster 2 at node 3 and into cluster 4 and cluster 5 at node 2; it also has the potential to differentiate into cluster 6 and cluster 7 at node 1, and cluster 7 may be the terminal cluster. The marker genes of clusters 1-7 are shown as a volcano plot and heatmap (Figure 1E, Figure S2A). The top 5 upregulated and top 5 downregulated signature genes of each cluster relative to other monocytes are labeled with different colors. Interestingly, some of the signature genes in cluster 1 and cluster 7 exhibited changes in the opposite direction. Specifically, *RETN*, *S100A8*, *S100A12*, and *S100A9* are among the 5 genes with the most upregulated signatures in cluster 1, while they are among the 5 genes with the most downregulated signatures in cluster 7. *FCGR3A* is among the 5 genes with the most downregulated signatures in cluster 1, while it is among the 5 genes with the most upregulated signatures in cluster 7. These findings suggest that the 2 clusters may have opposite biological functions. Human monocytes were divided into 3 subsets based on the leukocyte differentiation antigens CD14 and CD16.[6] At the transcriptional level, *CD14* and *CD16* may also play a role in distinguishing clusters. Therefore, we paid special attention to expression of *CD14* and *CD16* (*FCGR3A*) in each cluster (Figure 1F and G). *CD14* was highly expressed in clusters 1-7. However, it is worth noting that during differentiation from cluster 1 to cluster 7, expression of *CD14* first increased and then decreased (Figure 1F and H). Clusters 1-6 barely expressed *FCGR3A*, while cluster 7 highly expressed *FCGR3A* (Figure 1G). In addition, there was a negative correlation between expression of *CD14* and that of *CD16* in cluster 7 (Figure 1H). According to the clustering method of Ziegler-Heitbrock et al., $CD16^+$ monocytes can be further divided into intermediate monocytes ($CD14^{++}$) and nonclassical monocytes ($CD14^+$) according to the expression level of the CD14 protein, but there was no obvious indication of stratification of CD14 expression at the transcriptional level in cluster 7; that is, the expression level of *CD14* mRNA in cluster 7 was relatively uniform. This uniform expression may be because there are no or few nonclassical monocytes in the bone marrow, and Smiljanovic et al. confirmed this conclusion by flow cytometry.[30] Therefore, clusters 1–6 of bone marrow monocytes are likely 6 subsets of classical monocytes, and cluster 7 is likely intermediate

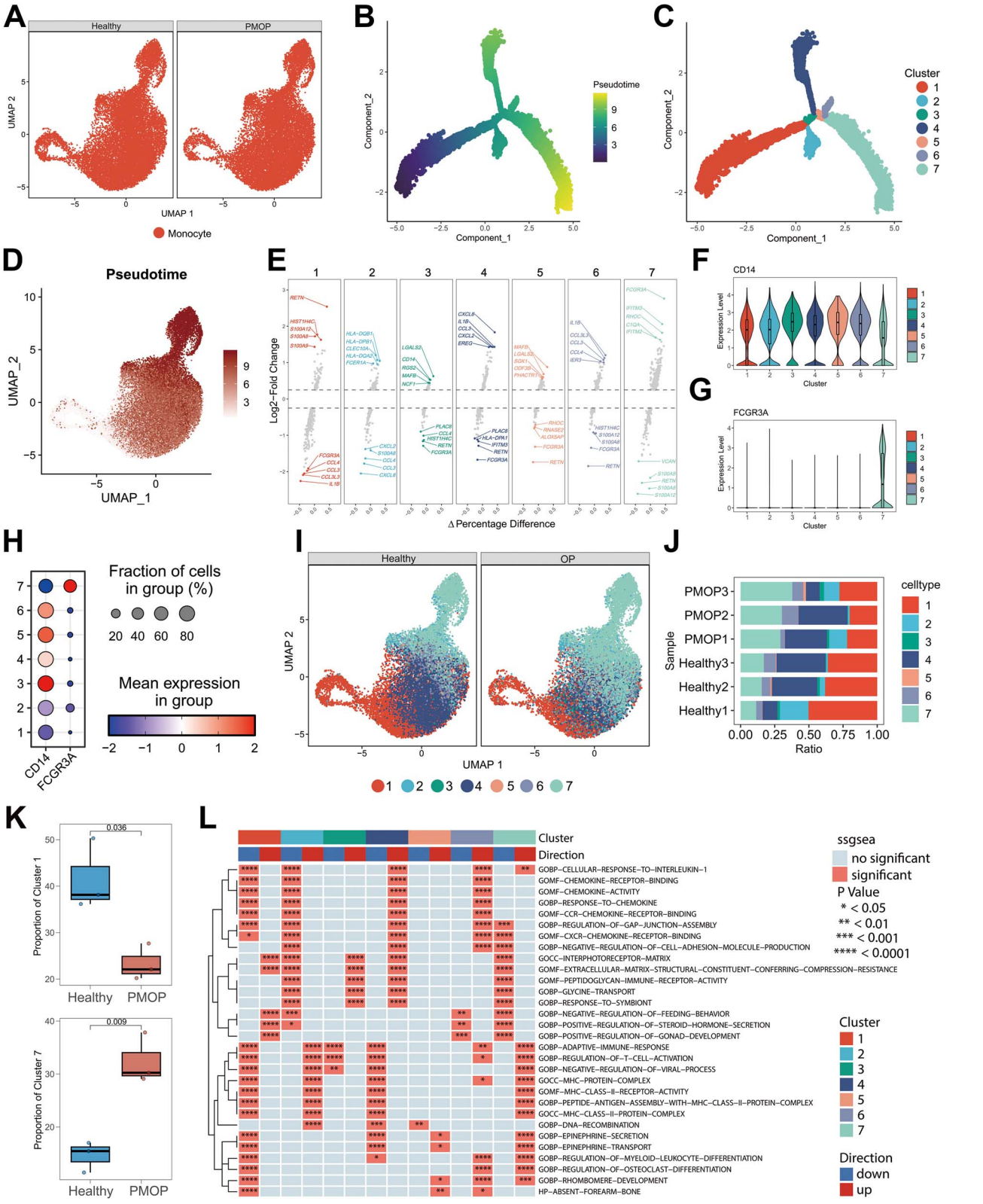

Figure 1. Changes in clusters of bone marrow CD14$^+$ monocytes in women with PMOP. (A) The distribution of bone marrow CD14$^+$ monocytes from postmenopausal women with normal bone mass in UMAP was highly similar to that from women with PMOP. (B and C) Results for Monocle2 analysis. (D) The pseudotime analysis results were mapped to UMAP; the lighter the color is, the more primitive the cell is. (E) Volcano plot of the marker genes in each cluster. The marker genes are provided as a "cluster.markers" file. (F) Expression levels of *CD14* mRNA in each cluster. (G) Expression levels of *FCGR3A* (*CD16*) mRNA in each cluster. (H) Average expression of *CD14* and *CD16* mRNAs in each cluster. (I) When the clusters were mapped to UMAP, the mapping positions of different clusters were similar, but there were differences in the proportion of clusters. (J) The stacked column chart of the proportions of 7 clusters in each sample. (K) The proportion of clusters 1 and 7 between healthy and PMOP samples. (L) The characteristic genes of each group were analyzed via GSEA.

monocytes. Although the proportion of each cluster has changed (Figure 1I), the monocyte distribution between the 2 groups on the UMAP was highly consistent (Figure 1A), suggesting that the overall expression patterns between the 2 groups were similar. In addition, the PCA dimension reduction algorithm was used to observe the grouping of the 7 clusters, and there was a great difference in gene expression patterns between cluster 1 and cluster 7 (Figure S2B). The proportion of cells in each cluster is shown in Figure 1J. The results showed that the main types of human bone marrow $CD14^+$ monocytes were cluster 1, cluster 4, and cluster 7. Compared with those of healthy postmenopausal women, the proportions of cluster 1 in PMOP women decreased significantly, the proportion of cluster 7 increased significantly (Figure 1K), and there was no difference in the proportion of clusters 2-6 (Figure S2C).

To understand the possible biological function of each monocyte cluster, the signature genes of each cluster were analyzed by GSEA, and the enrichment results are shown in Figure 1L. It is worth noting that the relationship between upregulation and downregulation of the pathways enriched by characteristic genes in cluster 1 and cluster 7 also showed some opposite characteristics; that is, some pathways downregulated in cluster 1 were upregulated in cluster 7. Specifically, "cellular response to interleukin 1", "apaptive immune response", "regulation of T-cell activation", "negative regulation of viral process", "MHC protein complex", "MHC class II receptor activity", "peptide antigen assembly with MHC class II protein complex", "MHC class II protein complex", "epinephrine secretion", "epinephrine transport", "regulation of myeloid leukocyte differentiation", "regulation of osteoclast differentiation", and "rhombomere development" were downregulated in cluster 1 and upregulated in cluster 7. A previous study has shown that the level of serum IL-1β in PMOP patients is significantly greater than that in healthy postmenopausal women.[31] IL-1 receptor antagonists can reduce bone loss and bone resorption in PMOP model rats.[32] MHC-II is distributed on the surface of antigen-presenting cells, including monocytes/macrophages, dendritic cells, and B-cells. After being processed into short peptides, extracellular proteins bind to MHC-II and are recognized by $CD4^+$ T-cells, thus activating the cells to become T helper 1 (Th1), Th2, Th17, Tfh, or Treg cells.[33] Activated T-cells produce IFN-γ, TNF-α, IL-17A, IL-4, and other cytokines,[34] which are important immune molecules involved in bone remodeling in PMOP.[35] In general, cluster 7 exhibited upregulated pathways related to inflammation, the immune response, and osteoclast differentiation, while cluster 1 exhibited the opposite trend, suggesting that cluster 7 may be involved in osteoporotic pathogenesis.

In addition, we applied single-cell regulatory network inference and clustering analysis to predict a variety of TFs with high activity in each cluster (Figure S2D). Based on the calculated regulon activity score of transcription factors, we identified differences in the activities of regulons among the cell clusters. SPI1, KLF7, and ZBTB7A, which promote osteoclast differentiation, exhibited high activity in cluster 7 and low activity in cluster 1.[36-38] To understand the metabolic landscape of $CD14^+$ monocytes in the bone marrow, the scores of all 75 active metabolic pathways in clusters 1–7 were computed (Figure S2E). There were significant metabolic differences between cluster 1 and cluster 7.

Developmental trajectory analysis of bone marrow $CD14^+$ monocytes

TSCAN was used to verify the conclusion of the differentiation direction of 7 clusters obtained by using Monocle2. The results of pseudotime analysis performed with the "TSCAN" package also support the conclusion (Figure 2A). VECTOR and scVelo were also used to verify the direction of differentiation among the 7 clusters, and the results were consistent with those obtained by using Monocle2 (Figure 2B and C). Compared with Monocle2 and VECTOR, scVelo has the advantage that its results represent the potential differentiation direction of cells at a certain moment rather than a coherent cell trajectory; hence, there is no need to use a priori knowledge of biology to specify the starting point and end point. In brief, we used different methods of analysis based on different theories to obtain the same results; thus, the results are robust.

We next attempted to analyze dynamic changes in expression of *CD14* and the top 10 upregulated characteristic genes in cluster 1 and cluster 7 during the differentiation of cluster 1 into cluster 7 in a pseudotime-dependent manner (Figure 2D). Levels of *ALOX5AP*, *HMGB2*, *RETN*, *RNASE2*, *HIST1H4C*, *STMN1*, *S100A9*, *LYZ*, *S100A8*, and *S100A12* decreased gradually during differentiation from clusters 1 to 7, while those of *CDKN1C*, *C1QA*, *FCGR3A*, *RHOC*, *IFITM2*, *MS4A7*, *HLA-DPB1*, *HLA-DPA1*, *LY6E*, and *IFITM3* increased gradually from clusters 1 to 7.

The proportion of cluster 7 of bone marrow monocytes increased in PMOP patients, and functional analysis of cluster 7 revealed that this increase is related to inflammation and osteoclast differentiation; these findings led us to wonder whether cluster 7 was the source of additional osteoclasts in PMOP patients. To this end, ssGSEA was used to analyze osteoclast scores with an osteoclast signature (https://www.genome.jp/entry/map04380) from the KEGG database, and osteoclast activity was calculated for each cell using ssGSEA. The osteoclast activity score increased gradually from cluster 1 to cluster 7 (Figure 2E and F), which indicated that cluster 7 was most similar to osteoclasts. These results suggest that cluster 7 may be the source of additional osteoclasts in PMOP patients.

Changes in the proportions of cluster 1 and cluster 7 were verified in unsorted bone marrow cells

The unsorted bone marrow cells from an additional 3 healthy postmenopausal women and an additional 3 women with PMOP were collected for scRNA-seq. After the initial quality control (Figure S3A–E), 28 477 cells were analyzed via single-cell transcriptome analysis. The single-cell resolution transcription landscape of the bone marrow samples from women with PMOP and healthy controls is shown in Figure S3F–H.

We isolated monocyte subsets from bone marrow cells, reduced dimensionality, and identified clusters 1 and 7 monocytes using AUCell (Figure 3A–E). The marker genes of clusters 1 and 7 are shown in Figure S3I. Moreover, VECTOR was used to reproduce the differentiation trajectory from cluster 1 to cluster 7 (Figure 3F). The proportion of cluster 1 monocytes in the PMOP patients was significantly lower than that in the healthy controls, while the proportion of cluster 7 monocytes was significantly greater (Figure 3G–I), which was consistent with the results of the bone marrow $CD14^+$ monocyte scRNA-seq analysis.

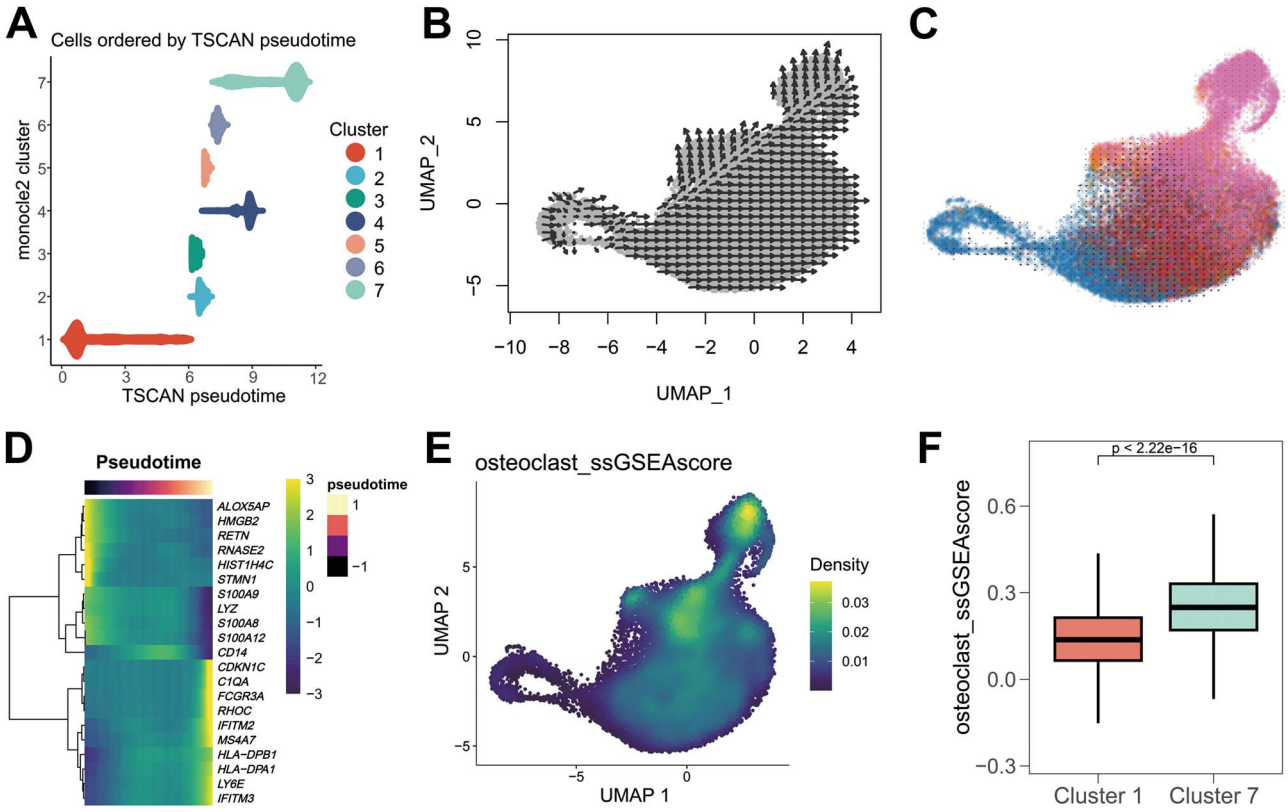

Figure 2. Developmental trajectory of bone marrow CD14^{+} monocytes. (A) Using the TSCAN package to perform pseudotime analysis, the smaller the abscissa value is, the more primitive the cell is. (B) Unsupervised inference of developmental directions for monocytes using VECTOR. (C) Map of the RNA velocity on UMAP. (D) Changes in dynamic expression of *CD14* and the top 10 upregulated characteristic genes in cluster 1 and cluster 7 during differentiation of cluster 1 into cluster 7 in a pseudotime-dependent manner. (E) Map of the osteoclast activity score on UMAP. (F) Boxplot of the osteoclast activity scores of clusters 1 and 7.

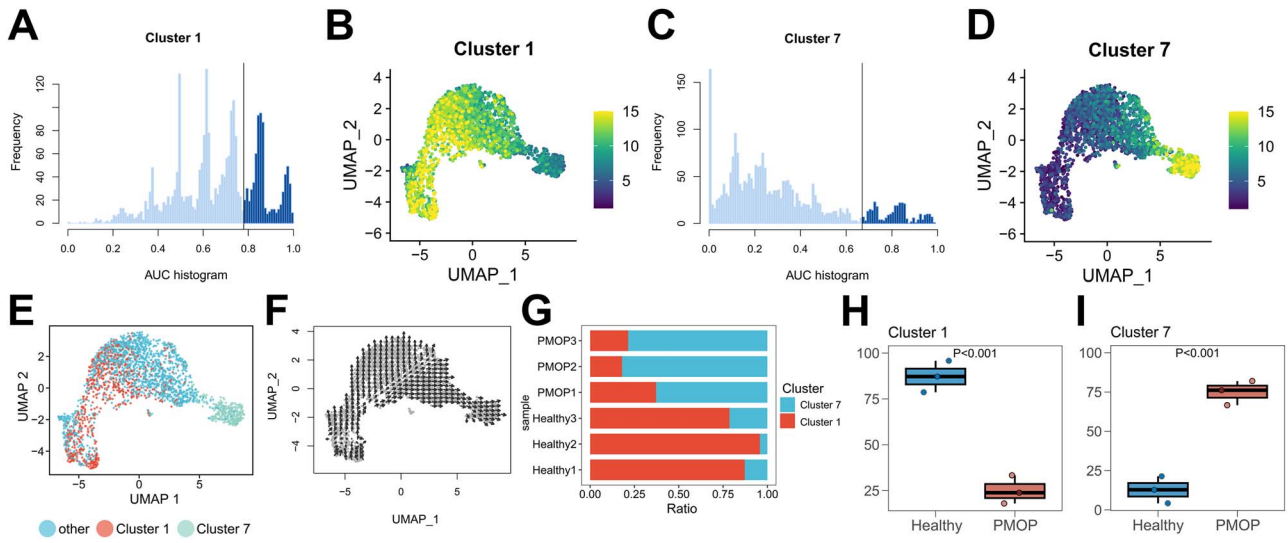

Figure 3. Changes in proportions of cluster 1 and cluster 7 in unsorted bone marrow. (A) Cluster 1 monocytes were identified by AUCell in unsorted bone marrow cells. (B) Mapping the AUC score of cluster 1 on the tSNE scatter plot. (C) Cluster 7 monocytes were identified by AUCell in unsorted bone marrow cells. (D) Mapping the AUC score of cluster 7 on the tSNE scatter plot. (E) Clusters 1 and 7 identified by AUC were mapped on the tSNE scatter plot. (F) Unsupervised inference of developmental directions for monocytes using VECTOR. (G) Stacked column charts of the proportions of clusters 1 and 7 of bone marrow *CD14*$^{+}$ monocytes in healthy postmenopausal women and women with PMOP. (H) Boxplot of the proportions of cluster 1 bone marrow *CD14*$^{+}$ monocytes in healthy postmenopausal women and women with PMOP. (I) Boxplot of the proportions of cluster 7 bone marrow *CD14*$^{+}$ monocytes in healthy postmenopausal women and women with PMOP.

Bulk transcriptome data did not detect differences, and genes in the same cluster were consistently expressed between the healthy and PMOP samples

PMOP is disease characterized by high bone turnover accompanied by increased osteoclast numbers in the bone and an increase in bone resorption during bone formation.[3] Under specific stimulation, circulating monocytes migrate to the bone and fuse with each other to form mature multinucleated osteoclasts.[39] However, differences in gene expression between the peripheral blood monocytes of women with PMOP and those of healthy postmenopausal women are surprisingly small. We performed PCA and generated a volcano plot of the DEGs based on bulk transcriptome data of peripheral blood monocytes from 20 postmenopausal women with high BMD and 20 postmenopausal women with low BMD from the GSE56815 dataset. PCA could not clearly distinguish between the 2 groups (Figure 4A), and there were few DEGs (Figure 4B). Similarly, we analyzed bulk RNA-seq data of peripheral blood monocytes from 5 postmenopausal women with high BMD and 5 postmenopausal women with low BMD from the GSE2208 dataset and obtained the same result (Figure 4C and D). The results of bulk transcriptome data showed that the overall gene expression of peripheral blood monocytes in women with PMOP was similar to that in healthy postmenopausal women. The value of traditional differential gene analysis in identifying the differences between 2 groups is limited, which may be due to the varying degrees of changes in the expression patterns of each subset; however, these changes have been minimized in the case of mixed gene sets. In addition, scRNA-seq data of bone marrow $CD14^+$ monocytes were grouped according to disease status, and the average gene expression in all cells of the healthy group and disease group was calculated by the AverageExpression () function of the Seurat package and then processed by $\ln(X+1)$. Expression in all cells in the healthy group was taken as the horizontal axis, and that in all cells in the disease group was taken as the vertical axis. The closer the diagonal is, the more equal the gene expression is; the difference is greater farther away from the diagonal. The results showed that after mixing the cells of all the clusters, all genes were basically close to the diagonal (Figure 4E), indicating that in the case of cluster mixing, a difference in gene expression between the 2 groups could not be observed, which was consistent with the results of the public bulk transcriptome data analysis. And then, pseudobulk analysis and DEseq2 were conducted to detect differences in clusters 1–7 between the 2 groups. In the 7 clusters, there were few DEGs between the healthy and PMOP groups. This indicates consistent gene expression in the same cluster in different groups (Figure 4F–L).

The change in the proportion of peripheral blood $CD14^+$ monocytes in cluster 1 and cluster 7 was similar to that of bone marrow monocytes in PMOP patients

Changes in the bone marrow are reflected in the peripheral blood. Peripheral blood monocytes may have a grouping pattern similar to that of bone marrow monocytes Thus, based on the characteristics of different cell states identified at the single-cell level, the "BayesPrism" R package was used to determine the different cell states of each sample in the GSE56815 dataset. Only protein-coding genes were retained and analyzed by the "new.prism" function. Figure S4 illustrates the quality control process employed for deconvolution. The results showed that a decrease in the proportion of cluster 1 and an increase in the proportion of cluster 7 peripheral blood monocytes are characteristic of PMOP and showed diagnostic value for PMOP (Figure 5A–D). To determine whether this result was biased by the algorithm, we used the top 10 marker genes for each cluster as the signature. We scored the cell content using the single sample gene set enrichment analysis (ssGSEA) method and obtained the same result (Figure 5E–H). The same analysis was applied to clusters 2–6, and the results are shown in Figure S5.

Because of the specific expression of *CD16* in cluster 7, to confirm the conclusion above, we collected peripheral blood from 10 women with PMOP and 10 healthy postmenopausal women. $CD14^+$ peripheral blood monocytes were separated by CD14 microbeads. Flow cytometry was performed to compare the proportions of $CD14^+CD16^-$ subsets and $CD14^+CD16^+$ subsets among $CD14^+$ peripheral blood monocytes between women with PMOP and postmenopausal healthy women. The results showed that the proportion of $CD14^+CD16^-$ cells among the peripheral blood monocytes of women with PMOP was significantly lower than that among the peripheral blood monocytes of healthy postmenopausal women, while the proportion of $CD14^+CD16^+$ cells was significantly greater (Figure 5I–K).

Cluster 1 and cluster 7 of bone marrow $CD14^+$ monocytes exhibit different cell–cell communications

Based on the knowledge of ligand/receptor pairs and other signal cofactors, CellChat can perform robust quantitative inference, analysis, and visualization of intercellular communication networks. We mainly described the communication networks involving cluster 1 and cluster 7 monocytes and scanned only those communication networks that do not involve them to predict the pathological changes in cell–cell communication associated with PMOP. We quantified and visualized the global communication map between clusters 1 and 7 of bone marrow monocytes and other cell groups by CellChat (Figure 6A). Clusters 1 and 7 of bone marrow $CD14^+$ monocytes exhibited cell–cell communication with almost all the other cell types (Figure 6B and C). We further investigated specific ligand–receptor interactions among the different cell clusters (Figure 6D and E). To determine the changes most likely to be associated with PMOP, we identified significantly different signaling pathways in cluster 1 and cluster 7. B-cells, NK cells, and other cell types had ligand–receptor interactions with CD4 in cluster 7 through the MHC class II antigen but lacked such interactions with 1 (Figure 6F, Figure S6A). A previous study showed that CD4–MHC-II stimulation of monocytes can promote differentiation of monocytes into macrophages and upregulate expression of proinflammatory cytokines and chemokines.[40] NK cells, pDCs, progenitor cells, T-cells, and B-cells have ligand–receptor interactions with CD4 in cluster 7 through IL16 but lack such interactions with those in cluster 1 (Figure 6G). Elssner et al. demonstrated that IL-16 signaling through CD4 activates the p38 MAPK and SAPK/JNK pathways in $CD4^+$ macrophages.[41] Selective inhibition of JNK was shown to result in the greatest decrease in IL-6 and TNF-α expression levels.[42] Cluster 1 exhibited strong ligand–receptor interactions with CAP1 in B-cells (Figure 6H), T-cells, and NK cells

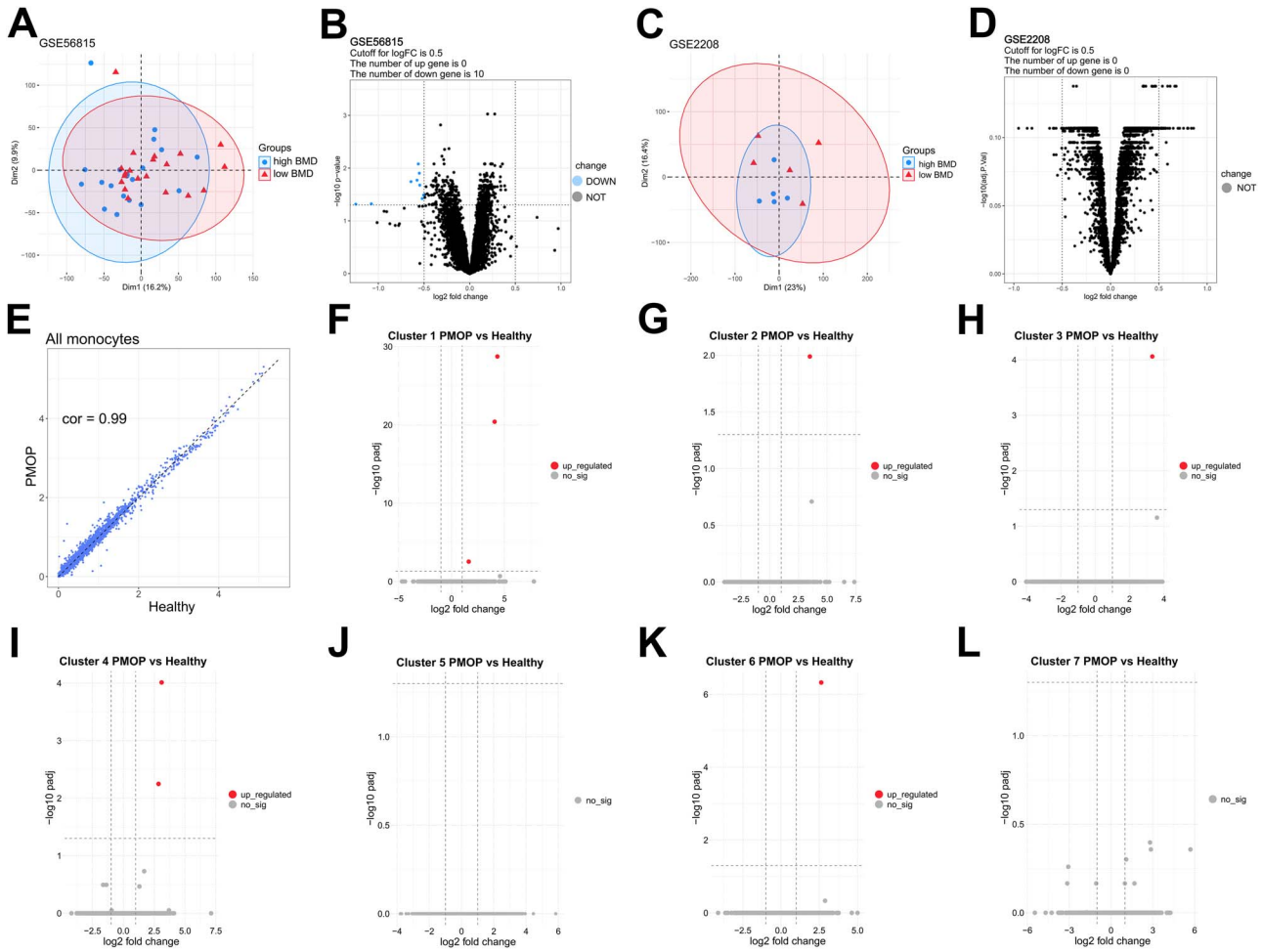

Figure 4. Bulk transcriptome data did not detect differences, and genes in the same cluster were consistently expressed between the healthy and PMOP samples. (A) PCA of bulk transcriptome data of peripheral blood monocytes from 20 postmenopausal women with high BMD and 20 postmenopausal women with low BMD in the GSE56815 dataset. (B) Volcano plot of bulk transcriptome data of peripheral blood monocytes from 20 postmenopausal women with high BMD and 20 postmenopausal women with low BMD in the GSE56815 dataset. (C) PCA of bulk transcriptome data of peripheral blood monocytes from 5 postmenopausal women with high BMD and 5 postmenopausal women with low BMD in the GSE2208 dataset. (D) Volcano plot of bulk transcriptome data of peripheral blood monocytes from 5 postmenopausal women with high BMD and 5 postmenopausal women with low BMD in the GSE2208 dataset. (E) The scatter plot of gene expression of each gene processed by ln (X + 1) in the scRNA-seq data of monocytes sorted by CD14 microbeads. (F–L) Volcano plot of 7 clusters.

through RETN. Resistin encoded by RETN is considered to be a proinflammatory factor.[43] However, there was no significant difference in resistin levels between women with PMOP and healthy individuals with normal BMD.[44] Several other ligand–receptor interactions with significant differences between Cluster 1 and Cluster 7 are shown in Figure S6B–I.

Discussion

Using scRNA-seq, we propose a method to classify the bone marrow CD14$^+$ monocytes of postmenopausal women into 7 clusters. The proportions of cluster 1 significantly decreased in the PMOP group compared with that in the healthy postmenopausal group, while the proportion of cluster 7 significantly increased. The function and metabolism of each cluster were characterized by ssGSEA, transcription factor analysis, and metabolic pathway analysis. We found that there were significant functional and metabolic differences between cluster 1 and cluster 7. Cluster 7 exhibited upregulated pathways related to inflammation, immunity, and osteoclast differentiation, while cluster 1 exhibited the opposite trend, suggesting that cluster 7 may be involved in osteoporotic pathogenesis. In addition, a decrease in the proportion of cluster 1 and an increase in the proportion of cluster 7 were verified in unsorted bone marrow cells.

We used Monocle2, TSCAN VECTOR, and scVelo to study differentiation relationship among the 7 clusters of bone marrow monocytes. Cluster 1 is the initial subset of differentiation, and cluster 7 is likely one of the terminal subsets of differentiation. These findings support Ziegler-Heitbrock et al.'s view that classical monocytes differentiate into intermediate and nonclassical monocytes.

By analyzing 2 bulk transcriptome datasets of peripheral blood monocytes in women with PMOP and healthy postmenopausal women, we propose that the cause of PMOP lies in the imbalance of monocyte subsets rather than changes in gene expression patterns. Changes in the proportions of clusters 1 and 7 are features of PMOP and have diagnostic value. This conclusion was confirmed using the peripheral blood

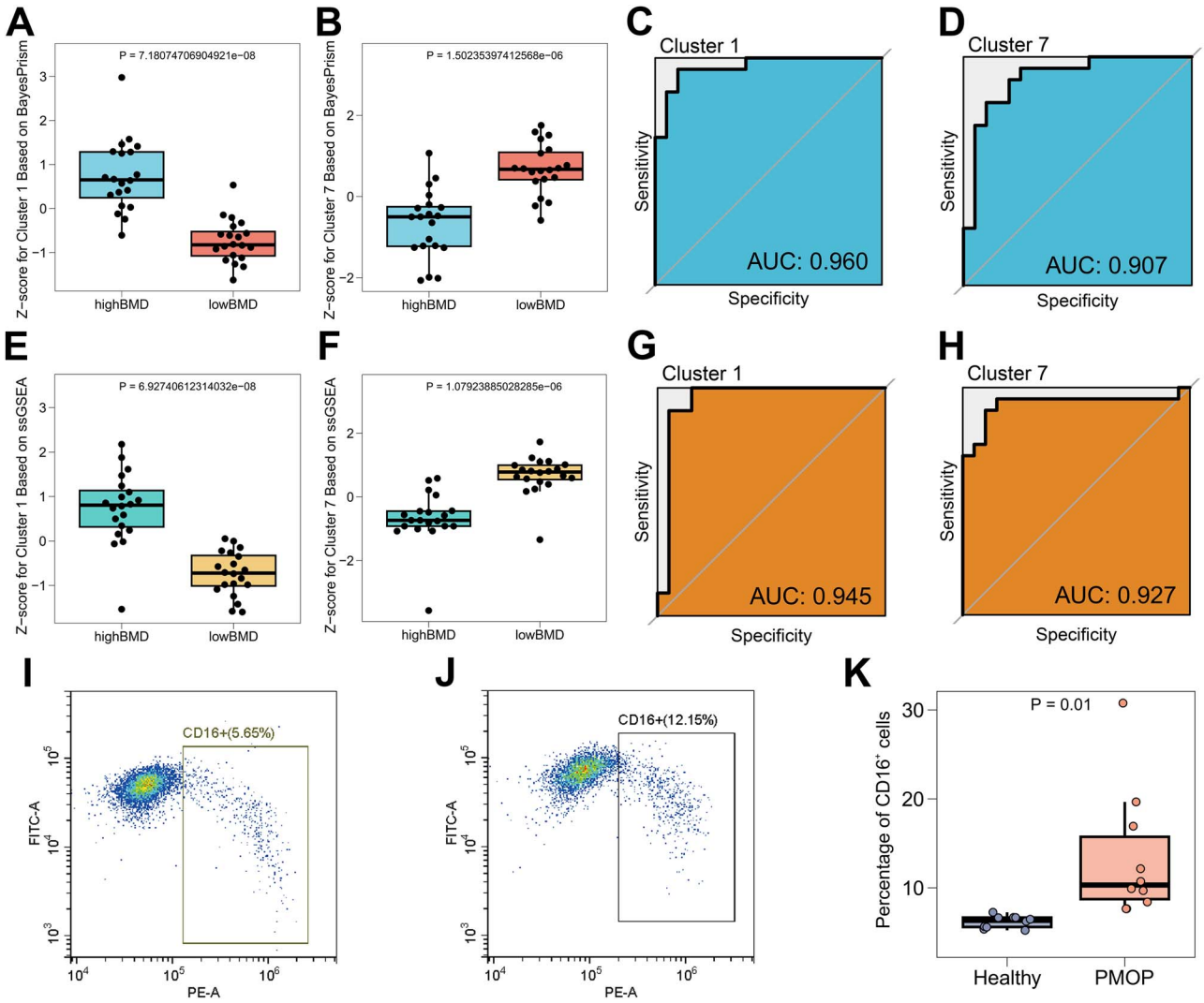

Figure 5. Changes in proportions of peripheral blood CD14$^+$ monocytes in cluster 1 and cluster 7. (A) The "BayesPrism" R package was used to determine the different cell clusters of each sample in the GSE56815 dataset. The z-score for cluster 1 of *CD14*$^+$ monocytes was greater in postmenopausal women with high BMD than in postmenopausal women with low BMD. (B) The z-score for cluster 7 of *CD14*$^+$ monocyte was lower in postmenopausal women with high BMD than in postmenopausal women with low BMD. (C) ROC curve of the z-scores for cluster 1 based on BayesPrism. (D) ROC curve of the z-scores for cluster 7 based on BayesPrism. (E) The z-score based on the ssGSEA) method for cluster 1 of *CD14*$^+$ monocytes was greater in postmenopausal women with high BMD than in postmenopausal women with low BMD. (F) The z-score based on the ssGSEA method for cluster 7 of *CD14*$^+$ monocyte was lower in postmenopausal women with high BMD than that in postmenopausal women with low BMD. (G) ROC curve of z-scores for cluster 1 based on ssGSEA. (H) ROC curve of z-scores for cluster 1 based on ssGSEA. (I) Expression of CD14 and CD16 in CD14$^+$ cells from postmenopausal women with normal BMD determined by flow cytometry. (J) Expression of CD14 and CD16 in CD14$^+$ cells from postmenopausal women with low BMD determined by flow cytometry. (K) The proportion of CD14$^+$CD16$^+$ cells in the peripheral blood of postmenopausal women with normal BMD or low BMD was determined by flow cytometry ($n = 10$ for normal BMD and $n = 10$ for low BMD). All flow cytometry results are provided as a "flow cytometry" file.

of 10 women with PMOP and 10 healthy postmenopausal women. In many studies, intermediate and nonclassical monocytes are classified as CD16$^+$ monocytes. One study has shown that changes in the composition of CD14$^+$CD16$^+$ and CD14$^+$CD16$^-$ monocytes lead to an increase in osteoclast formation in inflammation-driven bone loss diseases.[45] The function of intermediate monocytes in chronic diseases is unclear, though their role in cancer, rheumatoid arthritis, HIV, and other diseases has been reported.[8] The proportion of CD14$^+$CD16$^+$ monocytes is also increased in patients with multiple myeloma with osteolytic osteopathy.[46] Therefore, CD16$^+$ monocytes are likely a candidate marker of osteolytic bone destruction.

In addition, we studied the cell–cell communication patterns among bone marrow cells. In particular, we characterized in detail differences in communication signals between monocytes and other cells. These results support the promotional effect of cluster 7 on inflammation and osteoclast differentiation.

In summary, this study used scRNA-seq to explain the pathological changes in monocytes in women with PMOP that could not be detected by bulk RNA-seq; that is, the proportion of cluster 1 and cluster 7 monocytes among healthy women and women with PMOP was reversed, the differentiation relationship of each monocyte cluster was clarified, and cluster 7 monocyte was determined to be more closely related to

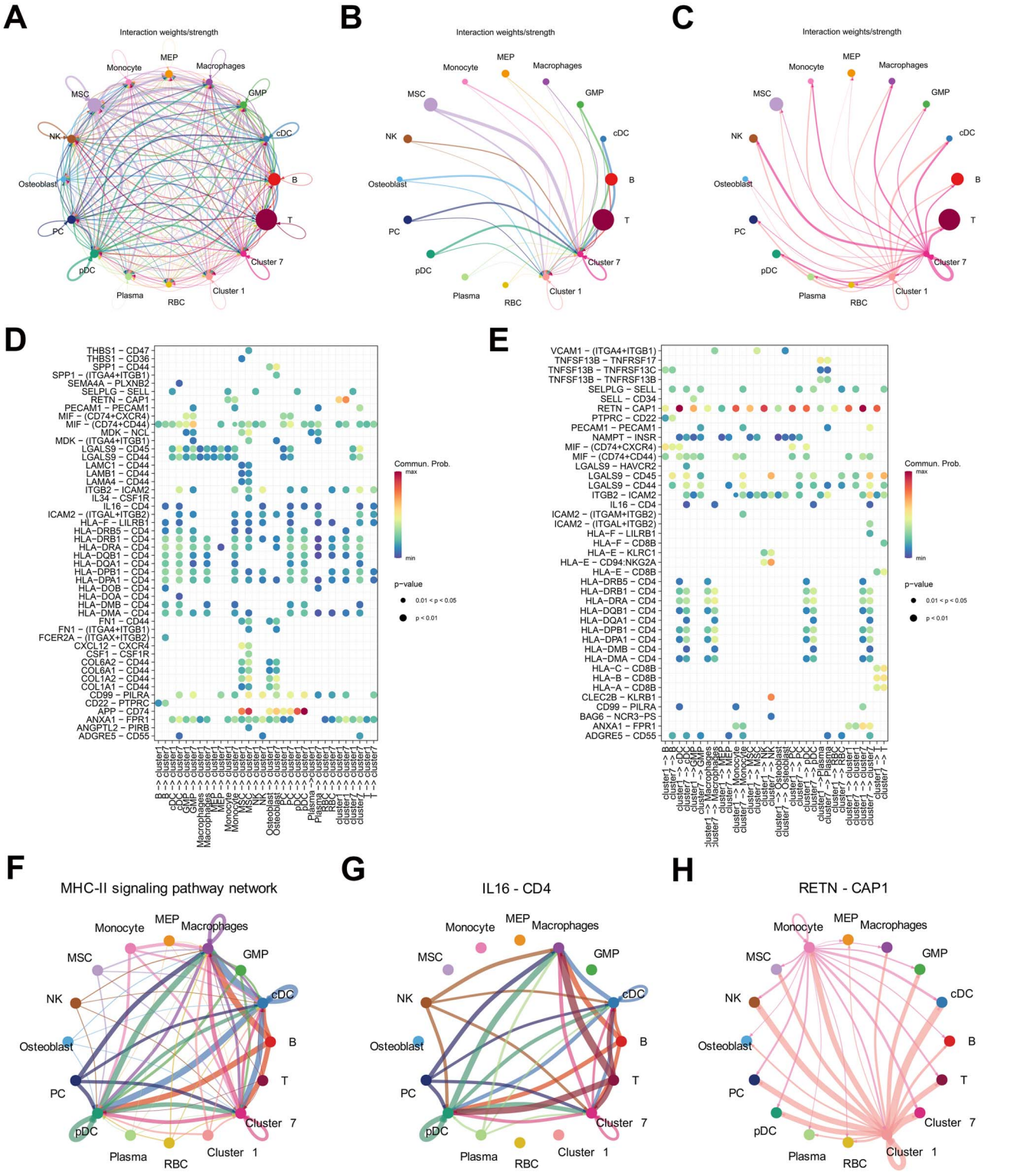

Figure 6. Cluster 1 and cluster 7 of bone marrow CD14^{+} monocytes exhibited different cell–cell communications. (A) CellChat was used to quantify and visualize the global communication map between clusters 1 and 7 of bone marrow CD14^{+} monocytes and other cell groups. (B) Clusters 1 and 7 widely received ligands from other cell groups. (C) Clusters 1 and 7 sent ligands to other cell groups. (D) Interaction between ligands emitted by different cell groups and specific receptors in clusters 1 and 7. (E) Interaction between specific receptors in clusters 1 and 7 and ligands emitted by different cell groups. (F) Cluster 1 lacks ligand–receptor interactions from other distinct cell groups with MHC-II as a ligand, while cluster 7 has the opposite effect. (G) Significant differences in IL-16-CD4 interactions between cluster 1 and cluster 7. (H) Significant differences in RETN-CAP1 interactions between cluster 1 and cluster 7.

osteoclasts. Our results suggest that inhibiting the overdifferentiation of cluster 1 monocytes into cluster 7 monocytes may be a new strategy for the prevention and treatment of PMOP.

Acknowledgments

We would like to thank all the volunteers who participated in this study. We thank Jingyuan Ning (Peking Union Medical College) for his advice on the scRNA-seq data analysis. We thank the nurses of the Department of Orthopedics of the First Hospital of China Medical University for their help in sample collection.

Author contributions

Lin Tao (Conceptualization, Data curation, Methodology, Writing—original draft), Wen Jiang (Methodology, Software, Validation, Visualization, Writing—original draft), Hao Li (Data curation, Software, Visualization, Writing—original draft), Zixuan Tian (Validation), Xiaochuan Wang (Validation), Keda Yang (Data curation, Resources, Validation), and Yue Zhu (Investigation, Supervision, Writing—review & editing).

All the authors have read and approved the final manuscript. First authors: Lin Tao, Wen Jiang, and Hao Li contributed equally to the work.

Supplementary material

Supplementary material is available at *Journal of Bone and Mineral Research* online.

Funding

This work was supported by the National Natural Science Foundation of China (32200943, 82072387) and the Shenyang Young and Middle-aged Science and Technology Innovation Talent Support Program (RC210171). The funding agencies played no role in the design of the study; the collection, or analysis, and interpretation of the data; or the writing of the manuscript.

Conflicts of interest

The authors declare that they have no competing interests.

Data availability

The raw sequence data reported in this paper have been deposited in the Genome Sequence Archive[47] in the National Genomics Data Center,[48] China National Center for Bioinformation/Beijing Institute of Genomics, Chinese Academy of Sciences (GSA-Human: HRA006095) that are publicly accessible at https://ngdc.cncb.ac.cn/gsa-human. All package information, codes, commands, and parameters used have been deposited in https://github.com/AcetylCoALab/bone/blob/main/pip.txt.

Ethics approval and consent to participate

The entire study was performed in the orthopedic and endocrine laboratories of the First Affiliated Hospital of China Medical University. The study was approved by the Ethics Committee of the First Affiliated Hospital of China Medical University (Research License 2019-142-2). All volunteers signed detailed informed consent forms and joined our research.

References

1. Wang L, Yu W, Yin X, et al. Prevalence of osteoporosis and fracture in China: the China osteoporosis prevalence study. *JAMA Netw Open*. 2021;4(8):e2121106. https://doi.org/10.1001/jamanetworkopen.2021.21106
2. Cummings SR, Melton LJ. Epidemiology and outcomes of osteoporotic fractures. *Lancet*. 2002;359(9319):1761–1767. https://doi.org/10.1016/S0140-6736(02)08657-9
3. Eriksen EF, Hodgson SF, Eastell R, Cedel SL, O'Fallon WM, Riggs BL. Cancellous bone remodeling in type I (postmenopausal) osteoporosis: quantitative assessment of rates of formation, resorption, and bone loss at tissue and cellular levels. *J Bone Miner Res*. 1990;5(4):311–319. https://doi.org/10.1002/jbmr.5650050402
4. Schett G. Cells of the synovium in rheumatoid arthritis. Osteoclasts. *Arthritis Res Ther*. 2007;9(1):203. https://doi.org/10.1186/ar2110
5. Udagawa N, Takahashi N, Akatsu T, et al. Origin of osteoclasts: mature monocytes and macrophages are capable of differentiating into osteoclasts under a suitable microenvironment prepared by bone marrow-derived stromal cells. *Proc Natl Acad Sci USA*. 1990;87(18):7260–7264. https://doi.org/10.1073/pnas.87.18.7260
6. Ziegler-Heitbrock L, Ancuta P, Crowe S, et al. Nomenclature of monocytes and dendritic cells in blood. *Blood*. 2010;116(16):e74–e80. https://doi.org/10.1182/blood-2010-02-258558
7. Wong KL, Tai JJ, Wong WC, et al. Gene expression profiling reveals the defining features of the classical, intermediate, and nonclassical human monocyte subsets. *Blood*. 2011;118(5):e16–e31. https://doi.org/10.1182/blood-2010-12-326355
8. Ozanska A, Szymczak D, Rybka J. Pattern of human monocyte subpopulations in health and disease. *Scand J Immunol*. 2020;92(1):e12883. https://doi.org/10.1111/sji.12883
9. Seeling M, Hillenhoff U, David JP, et al. Inflammatory monocytes and Fcγ receptor IV on osteoclasts are critical for bone destruction during inflammatory arthritis in mice. *Proc Natl Acad Sci USA*. 2013;110(26):10729–10734. https://doi.org/10.1073/pnas.1301001110
10. Sprangers S, Schoenmaker T, Cao Y, Everts V, de Vries TJ. Different blood-borne human osteoclast precursors respond in distinct ways to IL-17A. *J Cell Physiol*. 2016;231(6):1249–1260. https://doi.org/10.1002/jcp.25220
11. Jevon M, Hirayama T, Brown MA, et al. Osteoclast formation from circulating precursors in osteoporosis. *Scand J Rheumatol*. 2003;32(2):95–100. https://doi.org/10.1080/03009740310000102
12. Stuart T, Satija R. Integrative single-cell analysis. *Nat Rev Genet*. 2019;20(5):257–272. https://doi.org/10.1038/s41576-019-0093-7
13. Satija R, Farrell JA, Gennert D, Schier AF, Regev A. Spatial reconstruction of single-cell gene expression data. *Nat Biotechnol*. 2015;33(5):495–502. https://doi.org/10.1038/nbt.3192
14. Wolock SL, Lopez R, Klein AM. Scrublet: computational identification of cell doublets in single-cell transcriptomic data. *Cell Syst*. 2019;8(4):281–291.e9. https://doi.org/10.1016/j.cels.2018.11.005
15. Korsunsky I, Millard N, Fan J, et al. Fast, sensitive and accurate integration of single-cell data with harmony. *Nat Methods*. 2019;16(12):1289–1296. https://doi.org/10.1038/s41592-019-0619-0
16. Dominguez Conde C, Xu C, Jarvis LB, et al. Cross-tissue immune cell analysis reveals tissue-specific features in humans. *Science*. 2022;376(6594):eabl5197. https://doi.org/10.1126/science.abl5197
17. Zheng SC, Stein-O'Brien G, Augustin JJ, et al. Universal prediction of cell-cycle position using transfer learning. *Genome Biol*. 2022;23(1):41. https://doi.org/10.1186/s13059-021-02581-y
18. Qiu X, Mao Q, Tang Y, et al. Reversed graph embedding resolves complex single-cell trajectories. *Nat Methods*. 2017;14(10):979–982. https://doi.org/10.1038/nmeth.4402
19. Zhang F, Li X, Tian W. Unsupervised inference of developmental directions for single cells using VECTOR. *Cell Rep*. 2020;32(8):108069. https://doi.org/10.1016/j.celrep.2020.108069

20. Bergen V, Lange M, Peidli S, Wolf FA, Theis FJ. Generalizing RNA velocity to transient cell states through dynamical modeling. *Nat Biotechnol*. 2020;38(12):1408–1414. https://doi.org/10.1038/s41587-020-0591-3
21. Wu Y, Yang S, Ma J, et al. Spatiotemporal immune landscape of colorectal cancer liver metastasis at single-cell level. *Cancer Discov*. 2022;12(1):134–153. https://doi.org/10.1158/2159-8290.CD-21-0316
22. Aibar S, Gonzalez-Blas CB, Moerman T, et al. SCENIC: single-cell regulatory network inference and clustering. *Nat Methods*. 2017;14(11):1083–1086. https://doi.org/10.1038/nmeth.4463
23. Andreatta M, Carmona SJ. UCell: robust and scalable single-cell gene signature scoring. *Comput Struct Biotechnol J*. 2021;19:3796–3798. https://doi.org/10.1016/j.csbj.2021.06.043
24. Davis S, Meltzer PS. GEOquery: a bridge between the Gene Expression Omnibus (GEO) and BioConductor. *Bioinformatics*. 2007;23(14):1846–1847. https://doi.org/10.1093/bioinformatics/btm254
25. Lê S, Josse J, Husson F. FactoMineR: an R package for multivariate analysis. *J Stat Softw*. 2008;25(1):1–18. https://doi.org/10.18637/jss.v025.i01
26. Ritchie ME, Phipson B, Wu D, et al. Limma powers differential expression analyses for RNA-sequencing and microarray studies. *Nucleic Acids Res*. 2015;43(7):e47. https://doi.org/10.1093/nar/gkv007
27. Chu T, Wang Z, Pe'er D, Danko CG. Cell type and gene expression deconvolution with BayesPrism enables Bayesian integrative analysis across bulk and single-cell RNA sequencing in oncology. *Nat Cancer*. 2022;3(4):505–517. https://doi.org/10.1038/s43018-022-00356-3
28. Barbie DA, Tamayo P, Boehm JS, et al. Systematic RNA interference reveals that oncogenic KRAS-driven cancers require TBK1. *Nature*. 2009;462(7269):108–112. https://doi.org/10.1038/nature08460
29. Jin S, Guerrero-Juarez CF, Zhang L, et al. Inference and analysis of cell-cell communication using CellChat. *Nat Commun*. 2021;12(1):1088. https://doi.org/10.1038/s41467-021-21246-9
30. Smiljanovic B, Radzikowska A, Kuca-Warnawin E, et al. Monocyte alterations in rheumatoid arthritis are dominated by preterm release from bone marrow and prominent triggering in the joint. *Ann Rheum Dis*. 2018;77(2):300–308. https://doi.org/10.1136/annrheumdis-2017-211649
31. Al-Daghri NM, Aziz I, Yakout S, et al. Inflammation as a contributing factor among postmenopausal Saudi women with osteoporosis. *Medicine*. 2017;96(4):e5780. https://doi.org/10.1097/MD.0000000000005780
32. Kimble RB, Vannice JL, Bloedow DC, et al. Interleukin-1 receptor antagonist decreases bone loss and bone resorption in ovariectomized rats. *J Clin Invest*. 1994;93(5):1959–1967. https://doi.org/10.1172/JCI117187
33. Swain SL, McKinstry KK, Strutt TM. Expanding roles for CD4(+) T cells in immunity to viruses. *Nat Rev Immunol*. 2012;12(2):136–148. https://doi.org/10.1038/nri3152
34. Raphael I, Nalawade S, Eagar TN, Forsthuber TG. T cell subsets and their signature cytokines in autoimmune and inflammatory diseases. *Cytokine*. 2015;74(1):5–17. https://doi.org/10.1016/j.cyto.2014.09.011
35. Wu D, Cline-Smith A, Shashkova E, Perla A, Katyal A, Aurora R. T-cell mediated inflammation in postmenopausal osteoporosis. *Front Immunol*. 2021;12:687551. https://doi.org/10.3389/fimmu.2021.687551
36. Carey HA, Hildreth BE 3rd, Samuvel DJ, et al. Eomes partners with PU.1 and MITF to regulate transcription factors critical for osteoclast differentiation. *iScience*. 2019;11:238–245. https://doi.org/10.1016/j.isci.2018.12.018
37. Chen C, Hu F, Miao S, et al. Transcription factor KLF7 promotes osteoclast differentiation by suppressing HO-1. *Front Genet*. 2022;13:798433. https://doi.org/10.3389/fgene.2022.798433
38. Xu X, Shobuike T, Shiraki M, et al. Leukemia/lymphoma-related factor (LRF) or osteoclast zinc finger protein (OCZF) overexpression promotes osteoclast survival by increasing Bcl-xl mRNA: a novel regulatory mechanism mediated by the RNA binding protein SAM68. *Lab Investig*. 2022;102(9):1000–1010. https://doi.org/10.1038/s41374-022-00792-w
39. Zhou Y, Deng HW, Shen H. Circulating monocytes: an appropriate model for bone-related study. *Osteoporos Int*. 2015;26(11):2561–2572. https://doi.org/10.1007/s00198-015-3250-7
40. Zhen A, Krutzik SR, Levin BR, Kasparian S, Zack JA, Kitchen SG. CD4 ligation on human blood monocytes triggers macrophage differentiation and enhances HIV infection. *J Virol*. 2014;88(17):9934–9946. https://doi.org/10.1128/JVI.00616-14
41. Elssner A, Doseff AI, Duncan M, Kotur M, Wewers MD. IL-16 is constitutively present in peripheral blood monocytes and spontaneously released during apoptosis. *J Immunol*. 2004;172(12):7721–7725. https://doi.org/10.4049/jimmunol.172.12.7721
42. Baranova IN, Kurlander R, Bocharov AV, et al. Role of human CD36 in bacterial recognition, phagocytosis, and pathogen-induced JNK-mediated signaling. *J Immunol*. 2008;181(10):7147–7156. https://doi.org/10.4049/jimmunol.181.10.7147
43. Suragani M, Aadinarayana VD, Pinjari AB, et al. Human resistin, a proinflammatory cytokine, shows chaperone-like activity. *Proc Natl Acad Sci USA*. 2013;110(51):20467–20472. https://doi.org/10.1073/pnas.1306145110
44. Shu L, Fu Y, Sun H. The association between common serum adipokines levels and postmenopausal osteoporosis: a meta-analysis. *J Cell Mol Med*. 2022;26(15):4333–4342. https://doi.org/10.1111/jcmm.17457
45. de Vries TJ, El Bakkali I, Kamradt T, Schett G, Jansen IDC, D'Amelio P. What are the peripheral blood determinants for increased osteoclast formation in the various inflammatory diseases associated with bone loss? *Front Immunol*. 2019;10:505. https://doi.org/10.3389/fimmu.2019.00505
46. Petitprez V, Royer B, Desoutter J, et al. CD14+ CD16+ monocytes rather than CD14+ CD51/61+ monocytes are a potential cytological marker of circulating osteoclast precursors in multiple myeloma. A preliminary study. *Int J Lab Hematol*. 2015;37(1):29–35. https://doi.org/10.1111/ijlh.12216
47. Chen T, Chen X, Zhang S, et al. The genome sequence archive family: toward explosive data growth and diverse data types. *Genomics Proteomics Bioinformatics*. 2021;19(4):578–583. https://doi.org/10.1016/j.gpb.2021.08.001
48. CNCB-NGDC Members and Partners. Database resources of the National Genomics Data Center, China National Center for bioinformation in 2022. *Nucleic Acids Res*. 2022;50(D1):D27–D38. https://doi.org/10.1093/nar/gkab951